Vehicle System Dynamics
International Journal of Vehicle Mechanics and Mobility
ISSN: (Print) (Online) Journal homepage: www.tandfonline.com/journals/nvsd20

Suspension parameter optimal design to enhance stability and wheel wear in high-speed trains

Xiangwang Chen, Longjiang Shen, Xiaoyi Hu, Guang Li & Yuan Yao

To cite this article: Xiangwang Chen, Longjiang Shen, Xiaoyi Hu, Guang Li & Yuan Yao (2024) Suspension parameter optimal design to enhance stability and wheel wear in high-speed trains, Vehicle System Dynamics, 62:5, 1230-1252, DOI: 10.1080/00423114.2023.2224905

To link to this article: https://doi.org/10.1080/00423114.2023.2224905

VEHICLE SYSTEM DYNAMICS
2024, VOL. 62, NO. 5, 1230–1252
https://doi.org/10.1080/00423114.2023.2224905

Suspension parameter optimal design to enhance stability and wheel wear in high-speed trains

Xiangwang Chen[a], Longjiang Shen[b], Xiaoyi Hu[c], Guang Li[a] and Yuan Yao [a]

[a]State Key Laboratory of Traction Power, Southwest Jiaotong University, Chengdu, People's Republic of China; [b]Bogie R&D Department, CRRC Zhuzhou Electric Locomotive Co., Ltd., Zhuzhou, People's Republic of China; [c]Railway Science & Technology Research & Development Centre, China Academy of Railway Sciences Corporation Limited, Beijing, People's Republic of China

ABSTRACT

Ensuring running stability and minimising wheel tread wear are critical factors for enhancing the dynamic performance of high-speed trains. As an efficient method for improving vehicle performances, previous studies on suspension parameter optimisation have not fully considered these two factors. It is essential to pay attention to stability at extreme wheel-rail contact states, and the wheel wear evolution needs to be revealed instead of investigating the wear performance only through an index like wear number. This research aims to investigate the stability/wear Pareto optimisation of bogie suspension parameters for a high-speed passenger train. Stability-related indices are defined as the lateral ride comfort index at low equivalent conicity and the bogie frame acceleration at high conicity. To represent the long-term wheel wear performance, a contact spreading index is proposed and combined with the wear number index. The key suspension parameters are optimised through the genetic algorithm NSGA-II. The obtained Pareto front clearly reveals the relationship between the objective functions. To meet different performance requirements, four distinct matching rules of the suspension parameters are summarised by employing clustering analysis. Finally, the applicability of the parameter matching rules is examined by analysing stability at different equivalent conicities and wheel wear evolution.

ARTICLE HISTORY
Received 7 December 2022
Revised 5 June 2023
Accepted 8 June 2023

KEYWORDS
Suspension parameter design; running stability; wear evolution; high-speed train; Pareto optimisation

1. Introduction

Ensuring the long-term service of high-speed trains requires significant attention to running stability and wheel wear. Lateral stability of railway vehicles is closely related to ride comfort of passengers and running safety against derailment. However, due to the inevitable variation in wheel-rail contact states caused by wheel-rail wear and track deformation, the vehicle stability may deteriorate, and abnormal vibrations may arise [1]. In addition, wheel wear problems become more prominent with increased vehicle speed and traffic volume, leading to various dynamic problems that disrupt regular operation [2]. Properly addressing these two issues is essential to ensure that the vehicle can operate

CONTACT Yuan Yao yyuan8848@163.com

with desirable comfort and safety while also controlling operation and maintenance costs. Advanced mechanisms and active suspension systems have been proposed to solve the problems of lateral stability [3–5] and wheel wear [6,7], but their numerous components, inconvenient maintenance, and high costs make them impractical for the widespread adoption in practical engineering. Another useful method for improving vehicle dynamic performances is wheel profile optimisation [8–10]. Nevertheless, a newly-designed wheel profile requires long-term experimental on-track tests to assess its overall performances, and the reprofiling strategy needs to be reformulated. In this regard, optimising passive suspension elements can be considered a more economical and efficient alternative.

Optimising bogie suspension parameters to enhance stability and wheel wear is a typical multi-objective optimisation design, in which the design variables are always interdependent, and the objective functions cannot achieve optimal values at the same time. Several recent studies have been carried out regarding the multi-objective optimisation of bogie suspension. Magalhaes et al. [11] optimised suspension characteristics and operational velocity of a light railway vehicle. The optimisation process intended not only to improve running safety and ride quality, but also to increase the vehicle availability. Bideleh et al. [12] investigated Pareto optimisation of bogie suspension components to reduce wheel-rail contact wear and improve passenger ride comfort. Two suspension system configurations and various operational scenarios were considered. Global sensitivity of bogie dynamics with respect to suspension parameters, and robustness of suspension parameter optimised values were analysed as well [13,14]. Jiang et al. [15] established a multi-parameter and multi-objective optimisation platform for an articulated monorail vehicle to optimise its curving dynamic performance, and dynamic indices, such as the wheel unloading rate, Sperling index, and wear index, were improved through the genetic algorithm. Pandey et al. [16] proposed a novel approach of multi-objective optimisation of the dynamic performance of a freight wagon fitted with three-piece bogies. The bolster suspension parameters were optimised based on a surrogate model that uses the radial basis function. Yao et al. [17] put forward the concept of robustness of hunting stability and performed suspension parameters optimisation based on a liner high-speed vehicle model. Two matching types of suspension parameters were obtained. Then, a suspension parameters design combined with the idea of frequency-dependent stiffness of the yaw damper was conducted [18].

The aforementioned studies indicate that the selections of design variables and objective functions vary significantly based on the type of railway vehicle and operational scenarios. For Chinese high-speed railway lines, where the radii of the curved tracks on the main lines are normally larger than 5000 m, severe dynamic problems about the curving performance are rarely reported. Therefore, running stability and wheel tread wear performance on tangent tracks deserve significant attention. However, the stability/wear Pareto optimisation of bogie suspension parameters has been rarely considered before. Studies on the improvement of lateral stability for different wheel-rail contact geometries through suspension parameter optimisation have been carried out, but most of them are based on linear models [5,17,19]. Moreover, the improvement of wheel wear mostly is demonstrated by observing the reduction of the wear number [12,14,20,21]. This cannot illustrate, however, the extent to which wear can be reduced by using optimised suspension parameters because the wheel wear evolution in real operation is not considered. This study aims to optimise bogie suspension parameters while considering the wear pattern of wheel profiles.

The stability/wear Pareto optimisation of bogie suspension parameters conducted in this study is based on a high-speed passenger train model established in the multibody dynamics software SIMPACK. Four objective functions and five design variables are determined, and the genetic algorithm NSGA-II is used to achieve the Pareto optimisation front. Then, the correlation between the objective function values in the Pareto front is analysed. To get a deeper understanding of the influence of suspension parameter matching on the dynamic performance, clustering analysis is conducted to obtain the parameter distribution with different emphases on stability and wear performances of the vehicle. Finally, four representative suspension parameter combinations are extracted, and their corresponding stability at different wheel-rail contact geometries, as well as the wheel wear evolution within a reprofiling cycle, are investigated to summarise their detailed lateral dynamic characteristics.

2. Vehicle system modelling

A MBS dynamics model of a high-speed passenger train is developed in the simulation software SIMPACK [22], as shown in Figure 1. The vehicle model consists of a carbody, two bogie frames, four wheelsets, and eight axle boxes. All these components have 6 degrees of freedom (DoFs) except for the axle boxes which only consider a rotation around the wheelset axle. The vehicle has two stages of suspensions. The primary suspension is a combination of axle box springs, rotating arms, and primary vertical dampers. The secondary suspension consists of air springs, lateral dampers, vertical dampers, yaw dampers, anti-roll bars, and lateral stoppers. The suspension components are modelled as force elements that are simplified to a certain extent while ensuring the correct dynamic response. All springs are modelled to have stiffness in all three directions, and anti-roll bars are modelled as torsional springs. The Maxwell model, which connects stiffness and damping elements in series, is used to represent the dampers. The nonlinear damping properties of the dampers and the nonlinear stiffness properties of the stoppers are considered.

The standard wheel and rail profiles designed for the vehicle are S1002CN and CHN60, respectively. The rail inclination is 1:40, and the track gauge is 1435 mm with the measurement position situated at 16 mm below the rail crown. The friction coefficient in the wheel-rail interface is set to 0.35. The normal contact problem is solved by Hertz theory, and the FASTSIM algorithm is employed to calculate the creep force at the contact patch [23]. As a basic boundary condition for railway vehicles, the track irregularity power spectrum measured in the Wuhan-Guangzhou mainline is used, as it effectively represents the general track irregularity level of Chinese high-speed rail and is widely used for the dynamic simulation of high-speed trains. The adaptive solver SODASRT2 provided in SIMPACK with a tolerance of 10^{-5} is chosen for the dynamic simulation.

3. Predominant dynamic performance index

Considering all running scenarios and performance indices during optimising bogie suspension parameters is impractical. Instead, focusing on the predominant dynamic indices in extreme operational scenarios as optimisation objectives can be an efficient approach, as the indices in normal scenarios always can be satisfied.

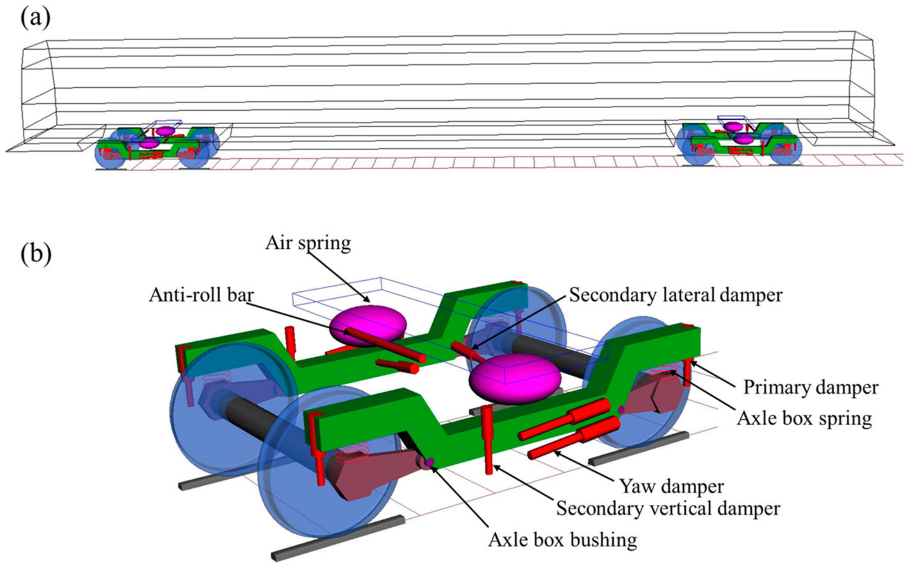

Figure 1. Vehicle system modelling: (a) one-car vehicle model; (b) bogie model.

3.1. Running stability

Due to the complicated environmental condition and variation of wheel-rail profiles, the equivalent conicity, regarded as a practical parameter to characterise the wheel-rail contact geometry, will vary greatly and has a significant influence on vehicle stability.

Figure 2 shows various wheel and rail profiles along with the corresponding equivalent conicity functions with respect to the wheelset lateral displacement. The equivalent conicity functions are calculated according to EN15302:2008 [24]. Different combinations of the wheel-rail profiles produce distinct contact geometries, leading to significant variations in the equivalent conicity curves. Rail grinding is a useful measure to correct the rail profile, control the generation and development of rail disease, and extend the rail service life. However, inadequate grinding accuracy can cause deviations from the standard profile, resulting in a poor wheel-rail matching relation. As depicted in Figure 2(b), the measured rail profile is excessively ground in the gauge corner, resulting in a wheel-rail contact equivalent conicity of about 0.06 at the wheelset lateral displacement of 3 mm when matched with the new wheel profile. This value is significantly lower than the standard wheel-rail matching equivalent conicity of about 0.18. Such a lower equivalent conicity can lead to the bogie hunting motion with a low frequency, approaching the natural frequency of the carbody. This can lead to carbody hunting instability [25,26], severely degrading ride comfort without exceeding the safety limit. Therefore, the lateral ride comfort of passengers at such a low equivalent conicity must be carefully addressed when designing suspension parameters. The Sperling index W, which is based on the measurement of carbody vibration acceleration, is widely used to quantify ride comfort and is defined as follows [27]

$$W = 3.57 \sqrt[10]{\frac{A^3}{f} F(f)} \tag{1}$$

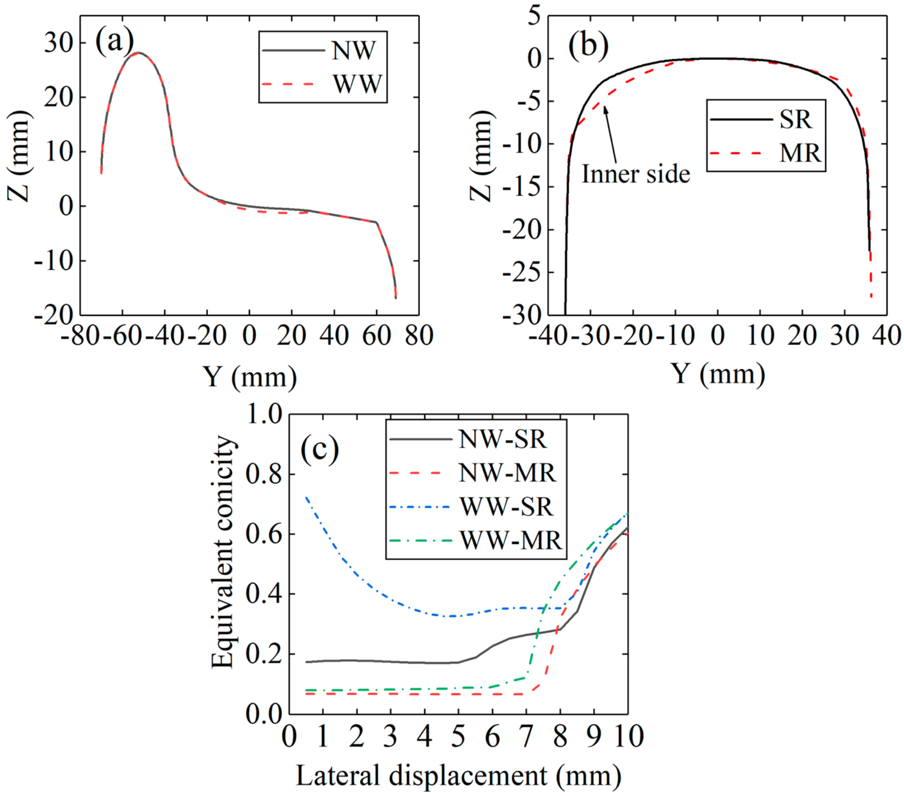

Figure 2. Wheel-rail profiles and contact geometries: (a) comparison of new wheel (NW) and worn wheel (WW) profiles; (b) comparison of standard rail (SR) and measured rail (MR) profiles; (c) wheel-rail contact equivalent conicity.

where A is the acceleration amplitude in the frequency domain, f is the corresponding frequency, and $F(f)$ is the frequency correction coefficient. For passenger vehicles, the limit values of ride comfort are 2.5, 2.75, and 3.0 for excellent, medium and qualified levels, respectively. Generally speaking, the excellent level is required during vehicle operation.

Conversely, wheel wear can result in a larger equivalent conicity at the later stage of a wheel reprofiling cycle. As shown in Figure 2(c), the equivalent conicity at the wheelset lateral displacement of 3 mm, obtained by the combination of the worn wheel and standard rail profiles, reaches a high value of about 0.38. This value increases even further when the matched rail profile is higher in the gauge corner [28]. Such a high equivalent conicity may cause bogie hunting instability, which is characterised by the violent lateral vibration of the bogie and can give rise to the instability alarm. Furthermore, if the frequency of the bogie hunting motion is sufficiently high and close to the frequency of the carbody elastic mode, the so-called carbody shaking phenomenon will arise and further worsen the ride comfort of passengers [29]. It is important to note that the equivalent conicity function exhibits a significantly negative slope around 3 mm, indicating that the vehicle will experience larger bogie frame accelerations compared to a positive slope with the same equivalent conicity at 3 mm [30,31]. Under this condition of high equivalent conicity, the bogie frame lateral acceleration is calculated according to the simplified measuring method defined in EN14363:2016 [32], in which the acceleration signal is firstly processed by the bandpass filter, and then the sliding root mean square (RMS) over 100 m distance with steps of 10 m of the resulting signal is computed. The maximum value of the sliding RMS values is defined as the dynamic performance index A_{high}.

3.2. Wear performance

Wheel wear is a critical issue that significantly affects vehicle performances and maintenance costs. A deep wear depth can shorten the wheel reprofiling mileage and increase operating costs. For Chinese high-speed trains, with the improvement of stability and ride comfort, wear often concentrates in the central area of wheel profiles due to the narrow wheel-rail contact band, leading to hollow wear as the main form of wheel wear. It can lead to bogie hunting instability and wheel-rail rolling contact fatigue [2]. Timely wheel reprofiling and rail grinding are commonly used countermeasures to deal with excessive hollow wear, but they are passive and costly. Therefore, this study aims to inhibit the development of wheel hollow wear from the perspective of suspension parameter design.

The distribution of wheel-rail contact points is regarded as an essential indicator of wheel wear, since local wear is assumed to be proportional to the frequency of contact point occurrence [33]. Polach [34] assumed that the stochastic wheelset displacement on lines with predominantly straight tracks could be represented by a normal distribution with a suited standard deviation. The wear spreading across the wheel tread profile was then determined by observing the distribution of corresponding wheel-rail contact points. The estimated wear of wheel profiles S1002, PF000, and PF602 showed good qualitative agreement with the measured results, particularly regarding the location of maximum wear and wear distribution asymmetry. Analogously, Figure 3 shows the probability distribution of contact point lateral positions on three typical wheel profiles used for Chinese high-speed trains, considering a standard deviation of wheelset lateral amplitude of 2 mm. The analysis suggests that the wear distribution of S1002CN is more even, while XP55 exhibits the most concentrated wear. Additionally, the wear distribution of S1002CN and LMA may be asymmetric, with the most-worn area located at the left and right sides of the nominal rolling circle, respectively. In summary, XP55 and LMA tend to develop hollow wear, while S1002CN is more prone to experience even lateral wear. These findings have been verified from field tests on the long-term wheel wear evolution [35,36]. However, it is important to note that the actual wheelset displacement may deviate from the normal distribution, and it can vary significantly for different combinations of wheel profiles and suspension parameters. Even for the same wheel profile, distinct suspension parameter matching also has a significant influence on the distribution of contact points. In order to simplify the characterisation of the contact point distribution and make a preliminary prediction of wheel wear, the contact spreading index (CSI) is defined, as shown in Equation (2).

$$\mathrm{CSI} = \frac{h}{w} \tag{2}$$

where w is the width of contact point distribution across the wheel profile, h is the maximum distribution probability of all contact positions, as shown in Figure 3. A smaller CSI indicates a less concentrated distribution of contact points, suggesting more uniform wheel wear. Conversely, a larger index value may suggest the occurrence of hollow wear. CSI is

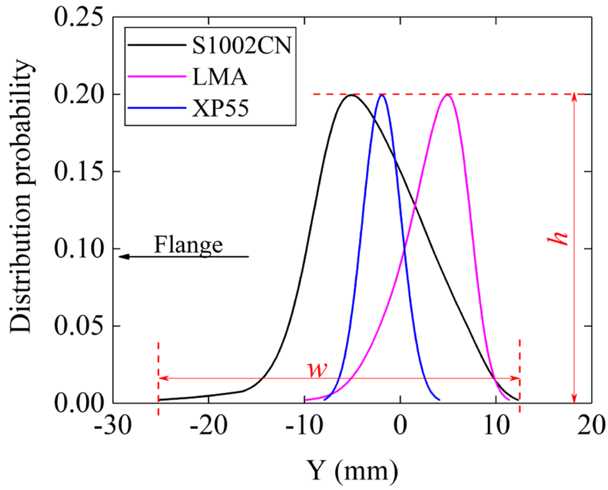

Figure 3. Distribution probability of contact point position on the wheel profile.

utilised as a useful index to represent wheel wear and is calculated based on the contact point distribution obtained from dynamic simulations.

In addition to the distribution of contact points, another common method to investigate wheel wear is based on the energy transfer model [37]. The energy dissipation within the contact patch is represented by the wear number, which is computed as the product of creep forces and their respective creepage. The wear number is widely used to quantify wheel wear and can effectively reflect the wear rate. Thus, a wear number index (WNI) is defined as follows:

$$\mathrm{WNI} = \int_{t_s}^{t_e} (T_x\gamma_x + T_y\gamma_y)\mathrm{d}t \tag{3}$$

where T_x is the longitudinal creep force, T_y the lateral creep force, γ_x the longitudinal creepage, γ_y the lateral creepage, t_s the simulation start time and t_e the end time. To reduce the removed wheel material, WNI should be kept as small as possible.

Typically, only one index is used in the evaluation of wheel wear performance, relying on either the contact point distribution or wear number. However, there may be instances where small wear numbers are accompanied by a concentrated distribution of contact points or the uniform contact point distribution coexists with large wear numbers. In such cases, predicting the development of wheel wear and drawing conclusions become changing. Therefore, CSI and WNI both are used in this study to conduct a comprehensive analysis. Smaller values of these indices indicate better wheel wear performance.

4. Multi-objective optimisation methodology

The settings of the stability/wear Pareto optimisation of bogie suspension parameters are introduced in this section, including design variables, objective functions, constraints, as well as the optimisation procedure.

Table 1. Design variables and optimisation ranges.

Parameters	Design ranges	Description
K_{px}	10–120 (kN/mm)	Longitudinal primary stiffness
K_{py}	3–20 (kN/mm)	Lateral primary stiffness
C_{sx}	200–2500 (kN·s/m)	Damping of the yaw damper
K_{ncsx}	5–40 (kN/mm)	Series stiffness of the yaw damper
C_{sy}	10–70 (kN·s/m)	Damping of the lateral secondary damper

Table 2. Objective functions and running scenarios.

		Scenarios			
Index	Unit	Speed (km/h)	Conicity	Wheel-rail matching	Description
W_{low}	/	250	0.06	NW-GR	Lateral ride comfort at low conicity
A_{high}	m/s^2	400	0.38	WW-SR	Bogie frame acceleration at high conicity
CSI	m^{-1}	300	0.18	NW-SR	Contact spreading index
WNI	J	300	0.18	NW-SR	Wear number index

4.1. Design variables

The number of design variables plays a vital role in the computational burden of multi-objective optimisation. The global sensitivity analysis makes it possible to recognise those suspension parameters that have the most significant influence on vehicle dynamics, thereby improving optimisation efficiency. Referring to the results obtained from the sensitivity analysis and parametric study [14,17,20,38], five suspension parameters are selected, including longitudinal primary stiffness K_{px}, lateral primary stiffness K_{py}, damping of the yaw damper C_{sx}, series stiffness of the yaw damper K_{ncsx}, and damping of the lateral secondary damper C_{sy}. The nonlinear damping properties of the damper are considered in the suspension parameter optimisation. The blow-off force of the damper remains fixed at its original value, while the blow-off velocity varies according to the damping coefficient. The parameter optimisation ranges are presented in Table 1 on the basis of the current values adopted by different types of high-speed trains in China.

4.2. Objective functions

As described in Section 3, four objective functions related to running stability and wheel wear performance are determined, and detailed simulation scenarios are presented in Table 2. The ride comfort index W_{low} at low equivalent conicity is calculated at a running speed of 250 km/h, because carbody hunting instability is usually more severe at a relatively low speed [25]. On the contrary, the calculation speed for the bogie frame acceleration at high equivalent conicity is set to 400 km/h to provide a stability margin. The analysis of the wear-related indices is conducted under the normal operational scenario.

4.3. Constraint functions

To ensure the curving performance of the vehicle, the derailment coefficient f_{de}, sum of wheelset lateral forces H, and wheel unloading rate η_{p} are checked during the suspension parameter design according to GB/T 5599–2019 [27]. Only the corresponding limit values are given here for the sake of brevity: $(f_{\text{de}})_{\max} = 0.8$, $(H)_{\max} = 58$ kN, and $(\eta_{\text{p}})_{\max} = 0.8$.

These safety indices are calculated for a curve with a radius of 5000 m and a cant deficiency of 90 mm, representing a severe operational scenario on curved tracks.

4.4. Formulation of the optimisation problem

The solution to a multi-objective optimisation problem involves finding a set of design variables such that none of the objective functions can be further improved without the deterioration in some of the remaining objective functions. Such design variable values are called Pareto optimal solutions, and the set of them is called the Pareto set. The objective function values corresponding to the Pareto set are referred to as the Pareto front. In this study, the optimisation problem aims to find design variable vectors $\mathbf{X} = [K_{px}, K_{py}, C_{sx}, K_{ncsx}, C_{sy}]$ between the upper bound **ub** and lower bound **lb,** to minimise the objective functions defined in Table 2. Meanwhile, the constraint functions must not exceed the limit values. The multi-objective optimisation problem can be described as follows:

$$\begin{cases} \text{Minimize:} \quad \{\, W_{\text{low}}, A_{\text{high}}, \text{CSI}, \text{WNI}\} \\ \text{Find:} \quad \mathbf{X} = [K_{\text{px}}, K_{\text{py}}, C_{\text{sx}}, K_{\text{ncsx}}, C_{\text{sy}}] \\ \text{Subject to:} \quad f_{\text{de}} \leq 0.8 \\ \eta_{\text{p}} \leq 0.8 \\ H \leq 58\text{kN} \\ \mathbf{l}b \leq \mathbf{X} \leq \mathbf{ub} \end{cases} \tag{4}$$

In order to solve the multi-objective optimisation problem, the Non-Dominated Sorting Genetic Algorithm (NSGA-II) with an elitist strategy is adopted [39]. This algorithm significantly improves the population diversity of solutions and computational efficiency. Three innovations, including the fast non-dominated sorting, crowding distance estimation, and simple crowded comparison operator, are introduced to get a more accurate Pareto front and reduce operational complexity. The algorithm starts with the initialisation of a random parent population of suspension parameter combinations. Only half of the population is selected based on non-domination rank and crowding distance to generate new suspension parameter combinations in the child population using genetic operator, crossover, and mutation. The parent and child populations are then combined into a single population to perform non-dominated sorting and generate new parameter combinations, ensuring the elitism of the best individuals. The optimisation iteration continues until the termination criteria or the maximum number of generations is reached. In the case that a constraint function is unsatisfied, all objective functions would be set to abnormally large values, guaranteeing that the parameter combination would not pass to the next generation. Considering the trade-off between the population diversity of solutions and computational burden, the population size is set to 1500 and the generation number is set to 12 in the NSGA-II algorithm.

The optimisation process is conducted through MATLAB/SIMPACK co-simulation. The NSGA-II algorithm is performed in the MATLAB environment, where the alternative design variables are generated and sent to the vehicle dynamic model for simulations in the SIMPACK environment. The simulation results obtained are then passed back to MATLAB, where the objective functions are evaluated to select Pareto optimal solutions.

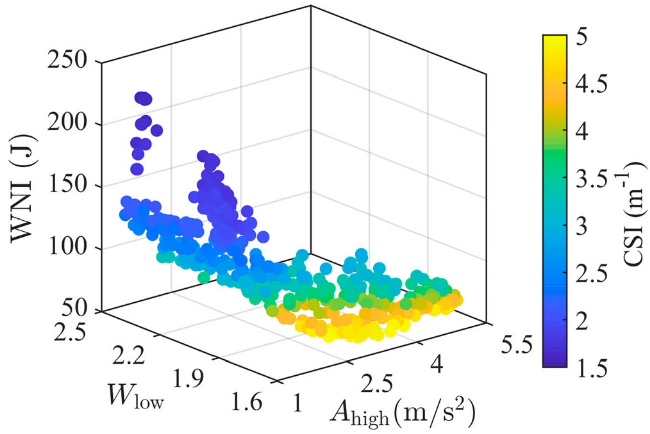

Figure 4. Stability/Wear Pareto front.

The communication between MATLAB and SIMPACK is realised through SIMPACK script languages, which are controlled by MATLAB to perform dynamic simulations and result outputs without requiring manual operation in the software interface. Finally, the optimisation procedure is terminated when the maximum number of iterations is reached.

5. Results and discussion

5.1. Pareto front

The Pareto front of the stability/wear optimisation is shown in Figure 4. The three coordinate axes represent the bogie frame acceleration A_{high} at high conicity, lateral ride comfort W_{low} at low conicity, and wear number index WNI, respectively. The smaller the index value, the better the corresponding dynamic performance. Besides, the colour of the data points represents the contact spreading index CSI, and the darker colour indicates a smaller index value, meaning that the distribution of contact points across the wheel profile is more uniform. The Pareto front illustrates the contradiction among the optimisation objects, and the Pareto optimal points have different emphases on the objective functions. According to different design requirements, the optimal suspension parameters corresponding to desired objective functions can be selected.

The two-dimensional projection of the Pareto front facilitates the observation of associations between the different objective functions. Figure 5 shows the correlations between W_{low} and the other indices. It can be observed that W_{low} has a negative correlation with A_{high} and CSI, and a positive correlation with WNI. Furthermore, it can be inferred that there is a positive correlation between A_{high} and CSI, and both of them show a negative correlation with WNI. The quantitative description of the correlations between the objective functions in the Pareto front is illustrated in Figure 6, using the Person's correlation coefficient [40]. This coefficient can range from -1 to $+1$, corresponding to the perfect negative correlation and perfect positive correlation, respectively. Significant associations are observed between the objective functions, particularly between WNI and CSI, where a highly strong negative correlation can be found. This indicates that a less concentrated distribution of contact points is usually accompanied by higher energy dissipation within the

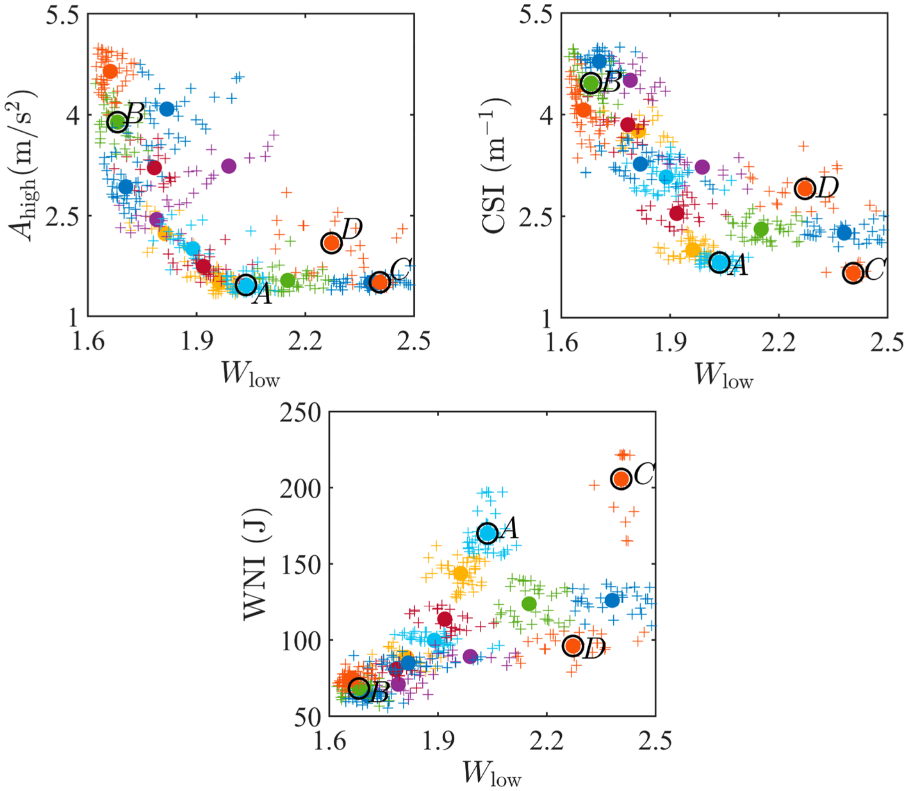

Figure 5. Two-dimensional projection of the Pareto front and clustering analysis.

contact patch and vice versa. The reason for this strong negative correlation is analysed in Section 5.3.2. The conflicting relationship between WNI and CSI highlights the limitation of selecting a single index to evaluate the wear performance of high-speed trains. In fact, for the vehicle that operates on lines containing many tight curves, using the wear number as the evaluation index is sufficient as the contact patch energy in the flange region contributes the most. However, for high-speed trains operating on lines with predominantly tangent tracks, determining which factor has the most crucial influence on wear accumulation is challenging due to the competition between the contact point distribution and contact patch energy.

5.2. Parameter matching analysis

According to different requirements for improving the dynamic performances, suspension parameter matching is investigated thereby. To handle the large amount of data in the Pareto front, clustering is applied to group closely related data points for further analysis. The self-organising map neural network [41] is used since it can always get stable clustering results. The obtained clustering results are shown in Figure 5, where adjacent data points with the same colour belong to the same cluster, and the highlighted points represent the cluster centres. Four representative clusters, labelled *A*, *B*, *C*, and *D*, are extracted for further study, as shown in Figure 5. The optimal objective functions of the four clusters are

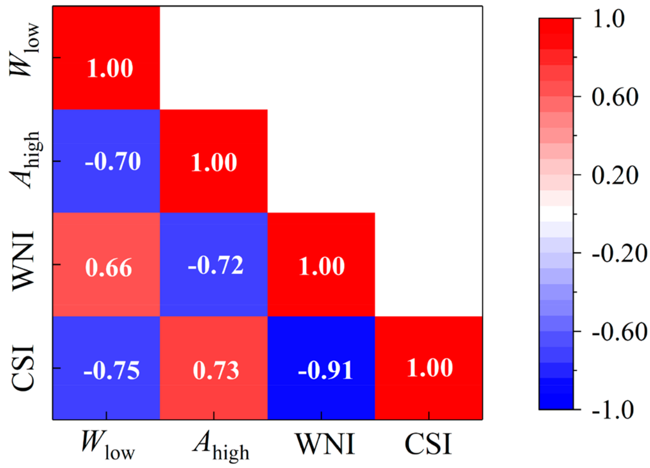

Figure 6. Heat map of correlation coefficients between the objective functions.

different. Cluster A has the best A_{high}, Cluster B has the best W_{low} and WNI, and Cluster C demonstrates the best CSI. Cluster D represents a trade-off among all optimisation objectives, resulting in more balanced performances.

Figure 7 displays the distribution of optimised suspension parameters for the four clusters using boxplots. Here the central red mark is the median value of the parameter data. The tops and bottoms of each rectangle represent the 25th and 75th percentiles, respectively, and the whiskers correspond to approximately 99.3 percent coverage of assumed normal distributed data. In addition, outliers beyond the whisker length are marked as red '+'. Matching rules of the suspension parameters can be summarised according to the different emphases on the optimisation objectives. It can be drawn from Figure 7 that K_{py} has minimal influence on the vehicle dynamic performances because the parameter distributions of the four clusters show slight variations. Cluster A adopts larger values of K_{px}, C_{sx}, and K_{ncsx}, contributing to enhanced high-conicity stability of the vehicle. Cluster B employs smaller K_{px} and K_{ncsx}, along with larger C_{sx}, leading to excellent lateral ride comfort at low conicity and small wear numbers. Cluster C exhibits concentrated parameter distributions with smaller C_{sx} and larger K_{ncsx} and C_{sy} chosen to achieve a more uniform distribution of wheel-rail contact points, albeit resulting in a larger wear number index. The dynamic performances of Cluster D are more comprehensive, for which smaller C_{sx} and C_{sy} are chosen, while the other suspension parameters are set to medium values. These four types of matching rules ought to be selected according to the practical engineering requirement. Notably, the parameter matching rules corresponding to Cluster B and D are in agreement with two types of high-speed trains in China, thereby validating the satisfactory effectiveness of the design method proposed in this study.

5.3. Applicability of parameter matching

Vehicle dynamic performances are analysed in detail by adopting the representative parameter combinations of the four clusters to assess their applicability. The specific values of the suspension parameters and corresponding optimisation indices are presented in Table 3.

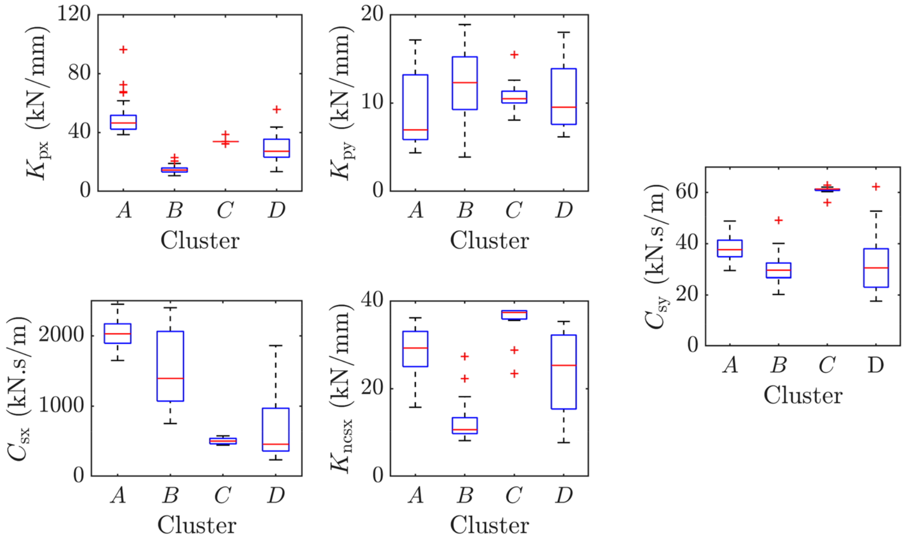

Figure 7. Suspension parameter distribution of the four clusters.

Table 3. Suspension parameter sets and corresponding objective function values.

	Suspension parameter					Objective function			
Cluster	K_{px} (kN/mm)	K_{py} (kN/mm)	C_{sx} (kN·s/m)	K_{ncsx} (kN/mm)	C_{sy} (kN·s/m)	W_{low}	A_{high} (m/s^2)	CSI (m^{-1})	WNI (J)
A	49.6	7.1	2169	27.2	38.4	2.03	1.47	1.83	176
B	15.3	9.2	1366	10.2	26.5	1.67	4.10	4.44	70
C	34.1	12.2	447	28.8	62.1	2.41	1.55	1.66	204
D	55.6	9.2	320	11.7	20.1	2.29	2.55	2.57	105

The running stability at different equivalent conicities and wheel wear evolution of the vehicle are investigated.

5.3.1. Stability with varying conicities

To investigate the vehicle stability under different wheel-rail contact geometries, the linear stability of the vehicle is studied by calculating the eigenvalues and eigenvectors of the system matrix in the state-space equation, where all nonlinearities associated with the suspension elements and wheel-rail contact are linearised. The damping ratio ζ and damped vibration frequency f of modes are defined as follows:

$$\eta = a + bi \tag{5a}$$

$$f = \frac{|b|}{2\pi} \tag{5b}$$

$$\zeta = \frac{a}{\sqrt{a^2 + b^2}} \tag{5c}$$

where i is the imaginary unit, η represents the eigenvalue of the system matrix, a and b are the real part and imaginary part of the eigenvalue, respectively. A negative value of a

indicates the modal vibration can be dampened, so the lateral instability occurs when ζ is greater than 0.

The root loci of the linear vehicle system are shown in Figure 8. They represent the variation in the modal damping ratio and damped vibration frequency with the equivalent conicity. Each root locus is composed of 29 sets of eigenvalues with the equivalent conicity varying from 0.04 to 0.6. Each 'o' represents a corresponding mode, and a larger symbol represents a higher conicity. The red symbols highlight the hunting mode with the maximum ζ at each equivalent conicity, which determines the stability margin of the vehicle system. The running speed is 300 km/h. From the figure, it can be observed that when the equivalent conicity is low, the linear stability of the vehicle is poor when adopting the suspension parameters from Cluster *A* and *C*. This indicates a high risk of carbody hunting instability, especially in the case of newly reprofiled wheel and improperly ground rail. However, as the equivalent conicity increases, the ζ corresponding to the hunting mode decreases, resulting in excellent lateral stability as the wheel wears. These two parameter combinations should be matched with a wheel profile with a higher equivalent conicity to avoid carbody hunting. The vehicle equipped with the suspension parameters from Cluster *B* exhibits better lateral stability under the low-conicity condition, but the stability deteriorates significantly when the equivalent conicity is high. To extend the wheel reprofiling cycle, a wheel profile with a lower conicity should be selected for the vehicle. Moreover, unlike the other parameter combinations where the system stability is determined by a single consecutive root locus of the hunting mode, the crucial mode for Cluster *B* experiences a sudden jump from a low-frequency carbody hunting mode to a high-frequency bogie hunting mode as the equivalent conicity increases. The parameter combination in Cluster *D* compromises extreme wheel-rail contact states, resulting in increasing vehicle stability with rising equivalent conicity, followed by a subsequent decrease. When the normal equivalent conicity is located at the turning position of the hunting root locus, the lateral stability is insensitive to the variation of wheel-rail contact geometry, and the vehicle would show strong adaptability to different railway lines.

The nonlinear stability of the vehicle is investigated through the bifurcation diagram of the wheelset lateral displacement with respect to the running speed, as shown in Figure 9, considering three wheel-rail profile combinations. Here only equilibrium solutions, including the stationary solution and stable limit cycle, are depicted, which is enough to determine the type of Hopf bifurcation and vehicle's critical speed.

As shown in Figure 9(a), the bifurcation analysis delivers a typical supercritical Hopf bifurcation when the vehicle adopts the low-conicity profile combination of NW-MR. A limit cycle oscillation occurs at a low speed, except for Cluster *B*, and the limit cycle amplitudes of Cluster *A* and *C* are larger than that of Cluster *D* when the running speed exceeds 200 km/h. It is important to note that with such a low-frequency oscillation, the safety limit value of bogie hunting instability is often not reached. Therefore, this behaviour is not regarded as unstable from the perspective of railway practice, but it significantly affects the running quality. Cluster *B* exhibits much better ride comfort than the other clusters, as shown in Figure 10(a), as it does not exhibit any limit cycle.

When the standard profile combination of NW-SR is adopted, the vehicle demonstrates a high critical speed under the normal-conicity condition. The stationary solutions of the four clusters overlap with each other. The nonlinear stability of Cluster *A* and *C* is excellent, with no limit cycle observed within the studied speed range, and their critical speeds have

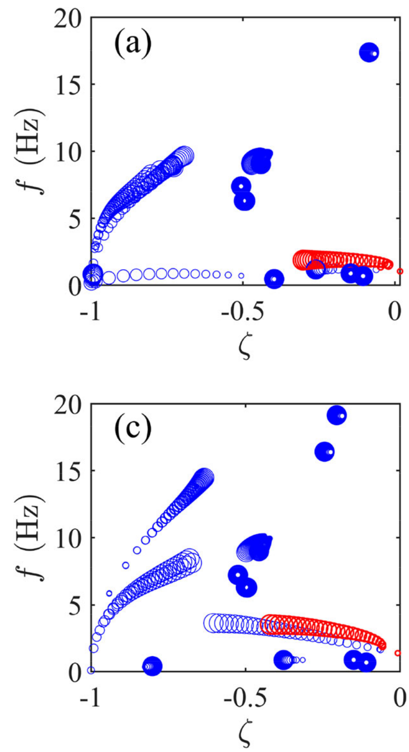

Figure 8. Root loci of the vehicle system with variation in equivalent conicity: (a) Cluster *A*; (b) Cluster *B*; (c) Cluster *C*; (d) Cluster *D*.

exceeded 900 km/h. The bifurcation types of Cluster *B* and *D* are different due to their distinct values of K_{px} and C_{sx}, which significantly affect the vehicle bifurcation behaviour [42,43]. Cluster *D* exhibits a subcritical bifurcation, in which the limit cycle oscillation with a large amplitude suddenly disappears as the vehicle speed falls below the nonlinear critical speed. Cluster *B* tends to display a supercritical bifurcation, and its limit cycle amplitude rapidly increases after surpassing the critical speed.

Under the high-conicity condition with the WW-SR profile combination, Cluster *A* and *C* show excellent nonlinear stability. Cluster *B* and *D* exhibit the supercritical bifurcation due to the negative slope of the equivalent conicity function [30]. Their critical speeds are approximately 400 km/h. However, the limit cycle amplitude of Cluster *B* is larger than that of Cluster *D* once the vehicle loses its stability. Therefore, Custer *B* may first reach the safety limit values due to the more severe bogie hunting.

The lateral ride comfort and bogie frame acceleration under the three conicity conditions are shown in Figure 10 for a detailed comparison. The vehicle running speed is 300 km/h. The indices can meet the requirements except for those of Cluster *C*. Its corresponding ride comfort index exceeds 2.5 at low and normal conicities, even though the bogie frame acceleration is well below the limit value. Cluster *C* achieves a wide distribution of wheel-rail contact points but at the expense of ride comfort. Thus, it cannot be adopted in practical applications. On the contrary, Cluster *B* demonstrates excellent dynamic performances at low conicity; however, its bogie frame acceleration under the high-conicity

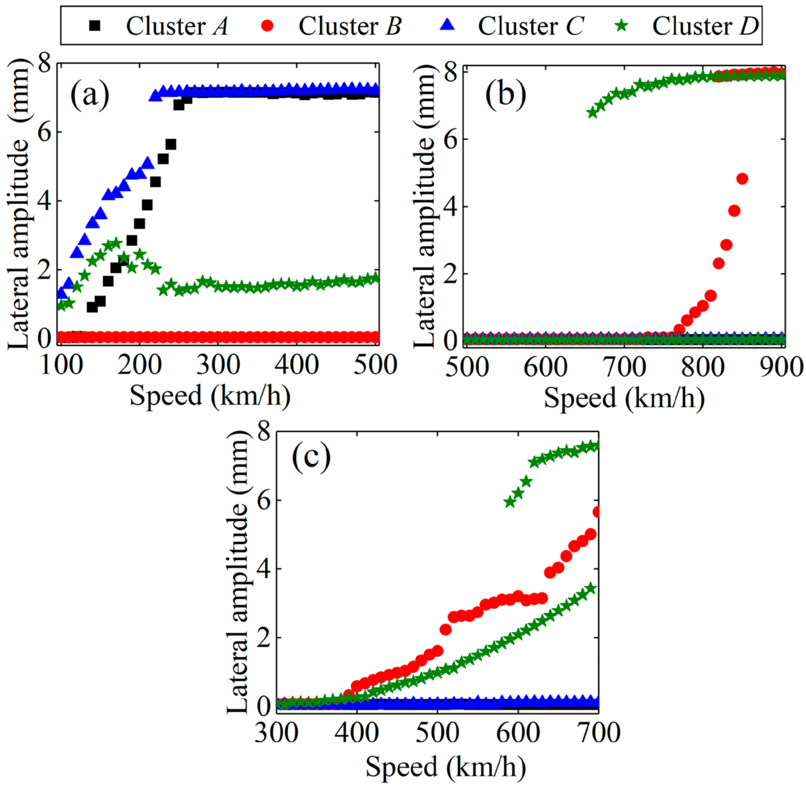

Figure 9. Bifurcation diagrams of wheelset displacement under different conicity conditions: (a) low conicity; (b) normal conicity; (c) high conicity.

condition is significantly larger than that of the other clusters, indicating a potential risk of bogie hunting instability at high speed and high conicity. Cluster *A* and *D* exhibit better adaptability to different wheel-rail contact geometries, as their corresponding indices remain satisfactory despite changing conicities. Furthermore, the lateral ride comfort of Cluster *D* is much better at normal conicity, making it the preferred choice for this type of high-speed train.

5.3.2. Wheel wear evolution

Figure 11 shows the distribution of wear numbers and lateral contact positions on the wheel tread profile for the four clusters. A small wear number indicates that the wheel-rail contact point is likely to be close to the nominal rolling circle, which explains the reason behind the strong negative correlation found between the wear number index WNI and contact spreading index CSI. The contact position far from the nominal rolling circle results in a large rolling radius difference, leading to increased longitudinal creepage and creep force, which contributes to higher wear numbers. This is true for almost all standard wheel-rail profile combinations, so the research finding can be extended to other wheel-rail combinations. Cluster *B*, which aims to minimise the wear number, can also bring about concentrated contact points around the nominal rolling circle, promoting the development of hollow wear. Cluster *A* and *C* have a wide distribution range of contact points, effectively

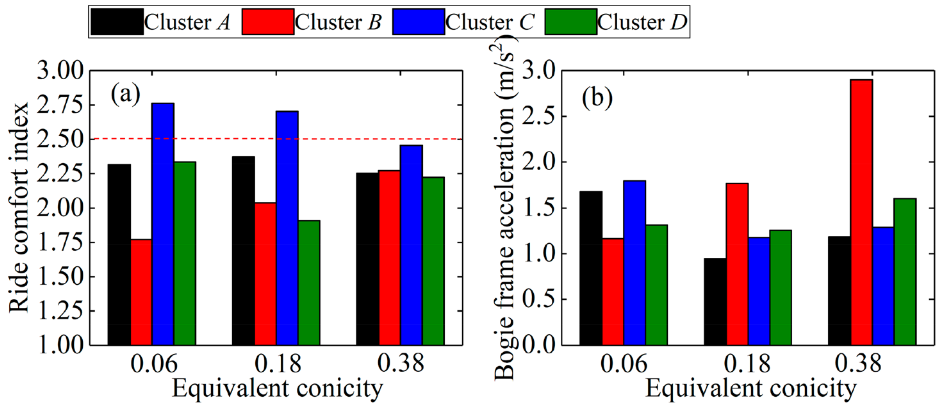

Figure 10. Lateral dynamic performances at different conicities: (a) lateral ride comfort; (b) bogie frame acceleration.

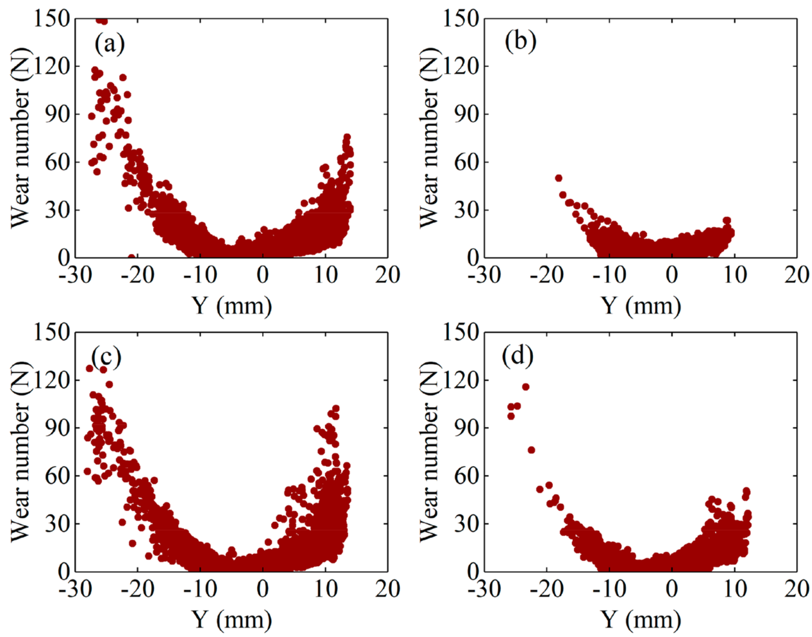

Figure 11. Distribution of wear number and contact position on wheel tread profile: (a) Cluster *A*; (b) Cluster *B*; (c) Cluster *C*; (d) Cluster *D*.

preventing the formation of hollow wear. However, the wear number at the contact point far from the nominal rolling circle is large, indicating the potential for deep wear. Cluster *D* shows significantly reduced wear numbers compared to Cluster *A* and *C*. Although the contact point distribution becomes narrower, it remains more uniform than that of Cluster *B*. Therefore, Cluster *D* achieves a desirable balance between the wear number and contact point distribution.

In order to clearly observe the wheel wear evolution, the wear simulation is executed based on the Archard model [44,45]. A statistical representation of typical curves and

Table 4. Track geometry properties of the high-speed railway line.

Radius (m)	Percentage (%)	Superelevation (mm)	Length of transition curve (m)	Length of circular curve (m)
5000	7	120	360	210
5500	7	165	360	210
7000	10	145	360	210
8000	8	120	340	250
9000	7	100	300	320
12000	1	80	220	480
∞	60	/	/	/

tangents that make up a Chinese high-speed railway line is used [46]. The geometry properties concerning seven different track segments are listed in Table 4. To reduce the simulation time without significantly affecting the results, the routine is assumed to be symmetric with respect to left and right curves, and the vehicle operates back and forth without turning at the final station. The updating strategy of the wheel profile during the iterative simulation is based on the travel distance. Once the mileage reaches 10,000 km the wheel profile is updated, and then the wear simulation will enter the next loop.

Figure 12 shows the wheel wear depth of the vehicle equipped with the four representative suspension parameter combinations after different operation mileages. The locations of maximum wear depths are all located at the left of the nominal rolling circle, consistent with the analysis from Figure 3. Cluster *B* has the smallest maximum wear depth for running distances less than 3×10^4 km, indicating that the wear number index can indeed reflect the wear performance within a relatively short distance. However, as the running distance increases, the wear depth of Cluster *B* increases significantly while maintaining a narrow wear width, exhibiting the typical characteristics of hollow wear. The wear patterns of Cluster *A* and Cluster *C* are similar in the first half of the whole operation cycle, but the wear depth of Cluster *C* grows faster than that of Cluster *A* during the later stage, despite having the widest wear range. More material needs to be removed to restore the worn tread profile to the standard shape although the economical reprofiling strategy is performed. This verifies that a single objective function based on either the wheel-rail contact point distribution or wear number cannot fully represent the long-term wheel wear performance, such as Cluster *B* and *C*. Notably, Cluster *D*, which makes a better balance between CSI and WNI, has the smallest wear depth after a longer travel distance. This indicates that the combination of medium CSI and WNI may benefit the wear performance. Furthermore, a comprehensive wear-related index that considers the contact point distribution and contact patch energy should be investigated in the future to fully reflect the wheel wear performance and facilitate the optimal design aimed at minimising the wear depth.

Figure 13 shows the detailed wheel wear evolution with the increasing travel distance by tracking wear depth and width changes. The difference in the maximum wear depths for the four clusters increases as the travel distance increases, and the wear rates also differ at different stages of the operation cycle. Cluster *C* consistently exhibits the largest wear depth after the travel distance exceeds 5×10^4 km, while Cluster *D* maintains the smallest wear depth. For instance, the maximum wear depth of Cluster *C* after running 25×10^4 km is 1.19 mm, while that for Cluster *D* is 0.79 mm, representing a decrease of 33.6%. Reasonable matching of the suspension parameters can significantly improve the wear performance.

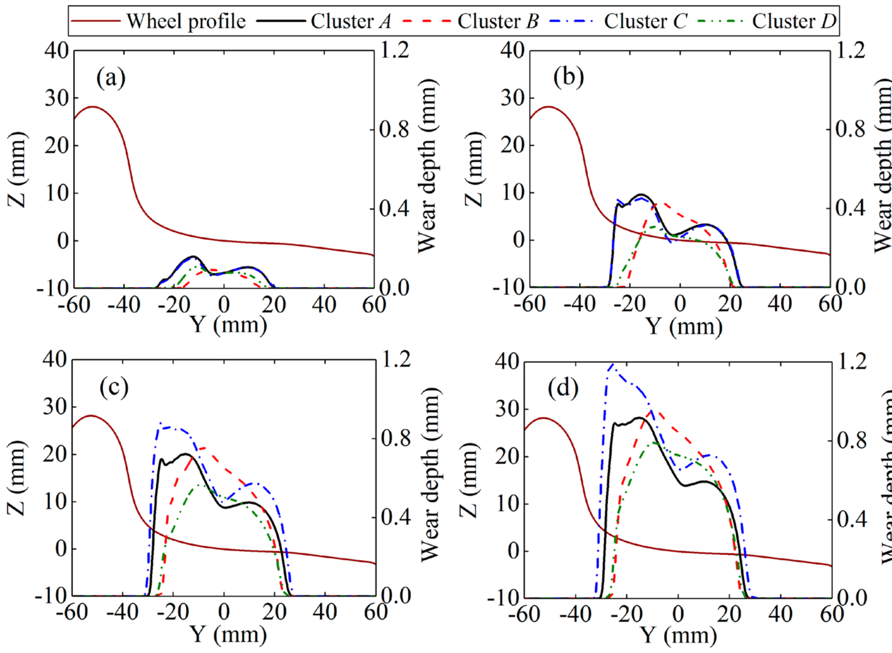

Figure 12. Tread wear distribution after different operation mileages: (a) 3 × 10^4 km; (b) 10 × 10^4 km; (c) 18 × 10^4 km; (d) 25 × 10^4 km.

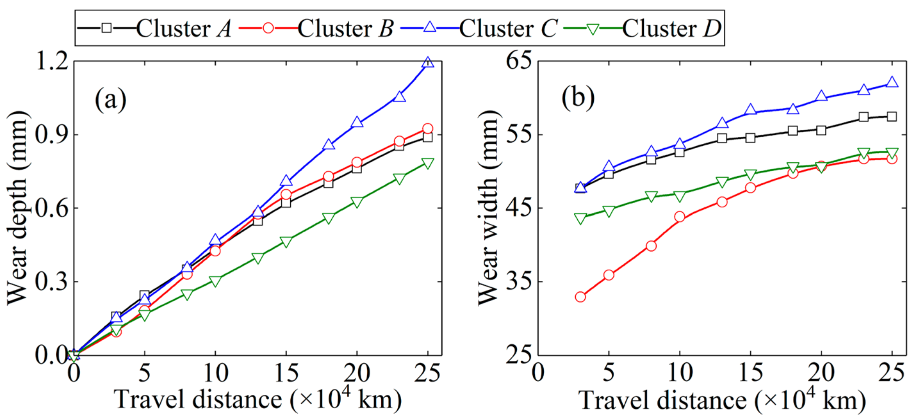

Figure 13. Tread wear evolution as functions of travel distance: (a) wear depth; (b) wear width.

The effective wear range of the tread profile gradually widens with the increase in the travel distance for Cluster *A*, *C*, and *D*, while Cluster *B* experiences a faster increase in the wear width during the early stage. The contact spreading index CSI can effectively represent the wear width, but it is not linearly proportional to the wear width throughout the operation cycle, especially in the later operation stage. Besides, there is no obvious relationship between the wear width and wear depth. A small wear width indeed accelerates the development of hollow wear, as observed in Cluster *B*, but a large wear width can lead to a deeper wear depth as well, as seen in Cluster *C*. Therefore, a moderate wear range may be more conducive to achieving a small wear depth and inhibiting hollow wear.

To summarise, the four clusters with distinct parameter matching yield significantly different lateral dynamic performances of the vehicle. Cluster *A* provides excellent high-conicity stability, but the corresponding normal-conicity ride comfort and wheel wear performance are relatively poor. Cluster *B* achieves the best low-conicity ride comfort but has the worst high-conicity stability with a tendency of wheel hollow wear. To obtain a less concentrated distribution of wheel-rail contact points and thereby inhibit hollow wear, Cluster *C* is selected; however, it results in the largest wear depth due to large wear numbers and poor lateral ride comfort regardless of the equivalent conicity. Cluster *D*, which considers all four performance indices, proves to be more suitable for the engineering application. It exhibits better adaptability to different wheel-rail contact geometries and provides the best wheel wear performance.

6. Conclusions

(1) A stability/wear Pareto optimisation method is proposed to enhance the lateral dynamic performance of a high-speed passenger train. Stability-related indices are defined as the lateral ride comfort W_{low} at low equivalent conicity and bogie frame acceleration A_{high} at high conicity to investigate the vehicle's adaptability to different wheel-rail contact geometries. To represent the wheel wear performance, the contact spreading index CSI is proposed to characterise the contact point distribution and combined with the wear number index WNI. The Pareto front obtained by using the genetic algorithm NSGA-II reveals the contradiction of the four objective functions. While W_{low} and WNI can be improved at the same time, A_{high} and CSI will deteriorate, and vice versa.

(2) The optimal combination of suspension parameters, including longitudinal primary stiffness K_{px}, damping of the yaw damper C_{sx}, series stiffness of the yaw damper K_{ncsx}, and damping of the lateral secondary damper C_{sy}, has a significant influence on the running stability and wheel wear performance of high-speed trains. Four distinct representative parameter matching rules are summarised, with different emphases on the lateral dynamic performances. Cluster *A* achieves excellent high-conicity stability by adopting larger values of K_{px}, C_{sx}, and K_{ncsx}. Cluster *B* provides better low-conicity ride comfort and small wear numbers by selecting smaller values of K_{px} and K_{ncsx}, and a larger value of C_{sx}. To obtain a more uniform distribution of contact points, Cluster *C* adopts a smaller value of C_{sx}, and larger values of K_{ncsx} and C_{sy}. The more balanced dynamic performances can be achieved by using the parameter combination of Cluster *D*, in which a smaller C_{sx} and C_{sy} are chosen, and the other suspension parameters are maintained at medium values.

(3) The applicability of the four parameter matching rules is investigated by analysing vehicle stability at different equivalent conicities and long-term wheel tread wear performance. Among the clusters, Cluster *D* is more suitable for the engineering application of this type of high-speed train. Its corresponding indices of lateral ride comfort and stability remain at satisfactory levels with different conicities, thus possessing good adaptability to changing wheel-rail contact states. Additionally, the best wheel wear performance is achieved by using the parameter combination of Cluster *D*.

(4) Using only the wear number to describe the wear performance is insufficient for the high-speed train operating on lines with predominantly tangent tracks because small wear numbers always lead to a concentrated distribution of contact points, accelerating the formation of wheel hollow wear. On the other hand, an excessively wide contact spreading can lead to a large wear depth as well. Therefore, reaching the balance between the wear number and contact point distribution can be beneficial for the wear performance. Furthermore, it is necessary to put forward a wear index that considers the influence of both contact patch energy and contact point distribution in further investigation. This will facilitate the wear performance evaluation and suspension parameter design.

Disclosure statement

No potential conflict of interest was reported by the author(s).

Funding

The material in this paper is based on work supported by the National Natural Science Foundation of China [grant number U2268211], the Natural Science Foundation of Sichuan Province [grant numbers 2022NSFSC0034; 2022NSFSC1901], and Independent Research and Development Project from State Key Laboratory of Traction Power [grant number [2022TPL_Q02].

ORCID

Yuan Yao http://orcid.org/0000-0003-2279-7463

References

[1] Li GD. Wheel-rail contact relation improvement and running adaptability for high speed emu. [PhD thesis]. Southwest Jiaotong University; 2019 [In Chinese].
[2] Zhai WM, Jin XS, Wen ZF, et al. Wear problems of high-speed wheel/rail systems: observations, causes, and countermeasures in China. Appl Mech Rev. 2020;72(6):060801. doi:10.1115/1.4048897
[3] Yao Y, Li G, Sardahi Y, et al. Stability enhancement of a high-speed train bogie using active mass inertial actuators. Veh Syst Dyn. 2019;57(3):389–407. doi:10.1080/00423114.2018.1469776
[4] Zhang XX, Wu GS, Li G, et al. Actuator optimal placement studies of high-speed power bogie for active hunting stability. Veh Syst Dyn. 2020;58(1):108–122. doi:10.1080/00423114.2019.1566556
[5] Zhang XX, Li H, Cheng J, et al. Adaptive stability mechanism of high-speed train employing parallel inerter yaw damper. Veh Syst Dyn. 2023. doi:10.1080/00423114.2022.2045027
[6] Tian SQ, Luo XP, Ren LH, et al. Active steering control strategy for rail vehicle based on minimum wear number. Veh Syst Dyn. 2021;59(8):1256–1281. doi:10.1080/00423114.2020.1743864
[7] Fu B, Hossein-Nia S, Stichel S, et al. Study on active wheelset steering from the perspective of wheel wear evolution. Veh Syst Dyn. 2022;60(3):906–929. doi:10.1080/00423114.2020.1838569
[8] Cui DB, Wang HY, Li L, et al. Optimal design of wheel profiles for high-speed trains. Proc Inst Mech Eng Part F J Rail Rapid Transit. 2015;229(3):248–261. doi:10.1177/0954409713509979
[9] Spangenberg U, Frohling RD, Els PS. Long-term wear and rolling contact fatigue behaviour of a conformal wheel profile designed for large radius curves. Veh Syst Dyn. 2019;57(1):44–63. doi:10.1080/00423114.2018.1447677
[10] Ye YG, Vuitton J, Sun Y, et al. Railway wheel profile fine-tuning system for profile recommendation. Railw Eng Sci. 2021;29(1):74–93. doi:10.1007/s40534-021-00234-1

[11] Magalhaes H, Madeira JFA, Ambrosio J, et al. Railway vehicle performance optimisation using virtual homologation. Veh Syst Dyn. 2016;54(9):1177–1207. doi:10.1080/00423114.2016.1196821
[12] Bideleh SMM, Berbyuk V, Persson R. Wear/comfort Pareto optimisation of bogie suspension. Veh Syst Dyn. 2016;54(8):1053–1076. doi:10.1080/00423114.2016.1180405
[13] Bideleh SMM. Robustness analysis of bogie suspension components Pareto optimised values. Veh Syst Dyn. 2017;55(8):1189–1205. doi:10.1080/00423114.2017.1305115
[14] Bideleh SMM, Berbyuk V. Global sensitivity analysis of bogie dynamics with respect to suspension components. Multibody Syst Dyn. 2016;37(2):145–174. doi:10.1007/s11044-015-9497-0
[15] Jiang YZ, Wu PB, Zeng J, et al. Multi-parameter and multi-objective optimisation of articulated monorail vehicle system dynamics using genetic algorithm. Veh Syst Dyn. 2020;58(1):74–91. doi:10.1080/00423114.2019.1566557
[16] Pandey M, Regis RG, Datta R, et al. Surrogate-assisted multi-objective optimization of the dynamic response of a freight wagon fitted with three-piece bogies. Int J Rail Transp. 2021;9(3):290–309. doi:10.1080/23248378.2020.1792808
[17] Yao Y, Li G, Wu GS, et al. Suspension parameters optimum of high-speed train bogie for hunting stability robustness. Int J Rail Transp. 2020;8(3):195–214. doi:10.1080/23248378.2019.1625824
[18] Yao Y, Chen XW, Li H, et al. Suspension parameters design for robust and adaptive lateral stability of high-speed train. Veh Syst Dyn. 2023;61:943–967. doi:10.1080/00423114.2022.2062012
[19] Sun JF, Chi MR, Jiao WD, et al. Modal parameters-based hunting stability analysis of high-speed railway vehicles considering full range of equivalent conicity. Proc Inst Mech Eng Part K J Multi-Body Dyn. 2022. doi:10.1177/14644193221103211
[20] Mazzola L, Alfi S, Bruni S. A method to optimise stability and wheel wear in railway bogies. Int J Railw. 2010;3(3):95–105.
[21] Johnsson A, Berbyuk V, Enelund M. Pareto optimisation of railway bogie suspension damping to enhance safety and comfort. Veh Syst Dyn. 2012;50(9):1379–1407. doi:10.1080/00423114.2012.659846
[22] SIMPACK 2018 Documentation. Dassault Systemes Simulia Corp, France; 2017.
[23] Iwnicki S, Spiryagin M, Cole C, et al. Handbook of railway vehicle dynamics. 2nd ed. Boca Raton (FL): CRC Press; 2020.
[24] EN 15302:2008+A1 – Railway applications – method for determining the equivalent conicity; 2010.
[25] Huang CH, Zeng J, Liang SL. Carbody hunting investigation of a high speed passenger car. J Mech Sci Technol. 2013;27(8):2283–2292. doi:10.1007/s12206-013-0611-z
[26] Li W, Guan QH, Chi MR, et al. An investigation into the influence of wheel-rail contact relationships on the carbody hunting stability of an electric locomotive. Proc Inst Mech Eng Part F J Rail Rapid Transit. 2022. doi:10.1177/09544097221084412
[27] GB/T 5599-2019. Specification for dynamic performance assessment and testing verification of rolling stock. National Railway Administration, People's Republic of China; 2019.
[28] Xu K, Feng Z, Wu H, et al. Investigating the influence of rail grinding on stability, vibration, and ride comfort of high-speed EMUs using multi-body dynamics modelling. Veh Syst Dyn. 2019;57(11):1621–1642. doi:10.1080/00423114.2018.1539234
[29] Chang C, Ding X, Ling L, et al. Mechanism of high-speed train carbody shaking due to degradation of wheel-rail contact geometry. Int J Rail Transp. 2023. doi:10.1080/23248378.2022.2077850
[30] Polach O. Characteristic parameters of nonlinear wheel/rail contact geometry. Veh Syst Dyn. 2010;48:19–36. doi:10.1080/00423111003668203
[31] Kulkarni R, Qazizadeh A, Berg M, et al. Investigating the effect of the equivalent conicity function's nonlinearity on the dynamic behaviour of a rail vehicle under typical service conditions. Veh Syst Dyn. 2022. doi:10.1080/00423114.2021.1962537
[32] EN 14363:2016+A1 – Railway applications – Testing and simulation for the acceptance of running characteristics of railway vehicles – Running behaviour and stationary tests; 2016.

[33] Polach O, Nicklisch D. Wheel/rail contact geometry parameters in regard to vehicle behaviour and their alteration with wear. Wear. 2016;366-367:200–208.
[34] Polach O. Wheel profile design for target conicity and wide tread wear spreading. Wear. 2011;271(1-2):195–202. doi:10.1016/j.wear.2010.10.055
[35] Shi HL, Wang JB, Wu PB, et al. Field measurements of the evolution of wheel wear and vehicle dynamics for high-speed trains. Veh Syst Dyn. 2018;56(8):1187–1206. doi:10.1080/00423114.2017.1406963
[36] Zhai WM, Liu PF, Lin JX, et al. Experimental investigation on vibration behaviour of a CRH train at speed of 350 km/h. Int J Rail Transp. 2015;3(1):1–16. doi:10.1080/23248378.2014.992819
[37] Pearce TG, Sherratt ND. Prediction of wheel profile wear. Wear. 1991;144(1-2):343–351. doi:10.1016/0043-1648(91)90025-P
[38] Li G, Wu RD, Deng XX, et al. Suspension parameters matching of high-speed locomotive based on stability/comfort Pareto optimization. Veh Syst Dyn. 2022. doi:10.1080/00423114.2021.1979602
[39] Deb K, Pratap A, Agarwal S, et al. A fast and elitist multi-objective genetic algorithm: NSGA-II. IEEE Trans Evol Comput. 2002;6(2):182–197. doi:10.1109/4235.996017
[40] Hollander M, Wolfe DA. Nonparametric statistical methods. Hoboken: Wiley; 1999.
[41] Kphonen T. The self-organizing map. Proc IEEE. 1990;78(9):1464–1480. doi:10.1109/5.58325
[42] Wu XW, Chi MR. Parameters study of Hopf bifurcation in railway vehicle system. J Comput Nonlin Dyn. 2015;10(3):0310123.
[43] Yan Y, Zeng J, Huang CH, et al. Bifurcation analysis of railway bogie with yaw damper. Arch Appl Mech. 2019;89(7):1185–1199. doi:10.1007/s00419-018-1475-6
[44] Archard JF. Contact and rubbing of flat surfaces. J Appl Phys. 1953;24(8):981–988. doi:10.1063/1.1721448
[45] Pires AC, Pacheco LA, Dalvi IL, et al. The effect of railway wheel wear on reprofiling and service life. Wear. 2021;477:203799. doi:10.1016/j.wear.2021.203799
[46] Huang CH, Luo R, Zeng J, et al. Effect of system parameters on tread-hollow wear of high-speed train wheels. J Traff Transp Eng. 2016;16(3):55–62. [In Chinese].